

Proving the stability estimates of variational least-squares kernel-based methods

Meng Chen^{a,b,c}, Leevan Ling^d, Dongfang Yun^e

^a*Department of Mathematics, Nanchang University, Nanchang, China*

^b*Institute of Mathematics and Interdisciplinary Sciences, Nanchang University, Nanchang, China*

^c*Xinjiang Vocational and Technical University of Tianshan, Kizilsu Kirgiz Autonomous Prefecture, Xinjiang, China*

^d*Department of Mathematics, Hong Kong Baptist University, Kowloon Tong, Hong Kong*

^e*School of Mathematics and Statistics, Central South University, Changsha, China*

Abstract

Motivated by the need for the rigorous analysis of the numerical stability of variational least-squares kernel-based methods for solving second-order elliptic partial differential equations, we provide previously lacking stability inequalities. This fills a significant theoretical gap in the previous work [Comput. Math. Appl. 103 (2021) 1-11], which provided error estimates based on a conjecture on the stability. With the stability estimate now rigorously proven, we complete the theoretical foundations and compare the convergence behavior to the proven rates. Furthermore, we establish another stability inequality involving weighted-discrete norms, and provide a theoretical proof demonstrating that the exact quadrature weights are not necessary for the weighted least-squares kernel-based collocation method to converge. Our novel theoretical insights are validated by numerical examples, which showcase the relative efficiency and accuracy of these methods on data sets with large mesh ratios. The results confirm our theoretical predictions regarding the performance of variational least-squares kernel-based method, least-squares kernel-based collocation method, and our new weighted least-squares kernel-based collocation method. Most importantly, our results demonstrate that all methods converge at the same rate, validating the convergence theory of weighted least-squares in our proven theories.

Keywords: Weighted Least-Squares Collocation, Numerical Stability, Convergence Theory.

AMS: 65N12, 65D15, 65N15

1. Introduction

In the early 1990s, E.J. Kansa [1] introduced a method to solve partial differential equations (PDEs) using the meshfree characteristics of radial basis function (RBF), which is generally referred to as kernel methods nowadays. Despite its adoption in various engineering and scientific applications, the theoretical foundations of the Kansa method were not established until well into the following decade. The initial theoretical backing attempts were unsuccessful until 2001 when Hon and Schaback [2] identified that the original Kansa method could experience failures in rare cases due to the singularity of the underlying linear system. Building on this, the author and his collaborators provided in 2006 [3] the first solvability results for a modified Kansa method that incorporated the idea of “overtesting”. This approach involved using a larger set of collocation points compared to the trial centers, resulting in an overdetermined system that required defining numerical solutions through a minimization process.

Further analysis by the author on the convergence in maximum norm of this overdetermined kernel collocation formulation [4] was published in 2008. In 2016, Schaback published a general framework for convergence proof and demonstrated that the convergence rate in the maximum norm could match that of the interpolant under specific smoothness conditions [5]. For computational sake, recent developments have seen the establishment of convergence theories for the least-squares minimizer in the overdetermined Kansa formulation [6].

Most recently, in 2021, Seyednazari *et al.* attempted to prove the convergence of a variational least-squares Kansa formulation. However, their published proof was found to be incomplete [7], indicating that there are still unresolved issues in fully validating this approach. Throughout the paper, we mainly follow the notations in [7] (hereafter referred to as “the referenced work”) for the sake of consistency, clarity, and to make the comparison of our results with those presented in the referenced work easy for readers. We consider second-order elliptic PDEs in a bounded domain $\Omega \subset \mathbb{R}^d$ subject to the Dirichlet boundary condition

$$\mathcal{L}u = f, \quad \text{in } \Omega, \quad (1a)$$

$$u = g, \quad \text{on } \partial\Omega, \quad (1b)$$

for a linear second-order uniformly elliptic operator

$$\mathcal{L}u := \sum_{i,j=1}^d a_{ij}(x) \frac{\partial^2 u}{\partial x_i \partial x_j} - \sum_{i=1}^d b_i(x) \frac{\partial u}{\partial x_i} - c(x)u,$$

with smooth and bounded coefficients. This paper addresses the need for a rigorous analysis of the numerical stability estimates of variational least-squares (VLS) kernel-based methods for solving second-order elliptic PDEs. Our analysis complements the analysis presented in the referenced work, which offered error estimates based on a conjecture [7, Eqn. 34] to prove the stability estimates. Our aim is to prove that, for any $0 \leq q \leq \tau - 2$, there exists a constant C such that the following stability estimate (referenced in Lemma 3.8 of the referenced work) holds:

$$C^{-1}h^{2q}\|u^h\|_{H^{q+2}(\Omega)}^2 \leq \|\mathcal{L}u^h\|_{L^2(\Omega)}^2 + h^{-3}\|u^h\|_{L^2(\partial\Omega)}^2, \quad (2)$$

for all trial function $u^h \in U_{\Phi,X}$ in the finite dimensional trial spaces $U_{\Phi,X}$ spanned by Sobolev space $H^\tau(\Omega)$ reproducing kernels Φ centered at the set of discrete data points $X \subset \Omega$ with fill distance $h = h_{X,\Omega}$. We provide a formal proof for the stability inequality without using the conjecture. By providing a rigorous proof of (2), we fill a significant gap in the existing literature and provide a comprehensive theoretical foundation for these methods.

In Section 2, we introduce necessary notations to ensure the stability result is understandable to readers and review the logical structure of error analysis concerning both continuous and discrete (i.e., collocation) least-squares kernel-based methods. Section 3 contains a formal proof of inequality (2). We also restate the resulting corollaries about error and condition number estimates, which are immediately valid given in our proof. Next, in Section 4, we prove another stability inequality involving weighted-discrete norms. This inequality is the key to the convergent analysis of a weighted least-squares (WLS) kernel-based collocation method. In Section 5, we compare these proven theoretical results of the various implementations of the method. This comparison provides insight into the relative efficiency and accuracy on data sets with large mesh ratio. We conclude in Section 6 with a discussion of implications and future work.

2. Assumptions and preliminaries

Given appropriate smoothness and boundedness assumptions on the domain Ω , the differential operator \mathcal{L} , and the data $f \in H^{k-2}(\Omega)$ and $g \in$

$H^{k-1/2}(\partial\Omega)$, we assume that the PDE (1) admits a classical solution $u \in H^k(\Omega)$ for some $k \geq 2$ and satisfies a boundary regularity estimate [8] of the form

$$\|u\|_{H^j(\Omega)} \leq C(\|f\|_{H^{j-2}(\Omega)} + \|g\|_{H^{j-1/2}(\partial\Omega)}) \quad \text{for } 2 \leq j \leq k. \quad (3)$$

In our previous proof for the error estimates involving least-squares kernel-based collocation methods for solving the PDE in (1), we made several standard assumptions, one being the boundary regularity in (3). Other assumptions involved the domain, differential operator, and solution characteristics, as outlined in Assumptions 2.1–2.4 of [6] (hereafter referred to as “our prior work”). In the referenced work focusing on VLS kernel-based methods, the authors assumed the PDE was of Agmon-Douglis-Nirenberg type [9], enabling them to assert the boundary regularity.

We work in some norm-equivalent Hilbert spaces $H^\tau(\Omega)$, with $\tau > d/2$ and $\tau \geq k$ the smoothness of the PDE solution, reproduced by some symmetric positive definite kernel Φ with translation-invariance whose Fourier transform decays algebraically as

$$C_1(1 + |\omega|_2^2)^{-\tau} \leq \widehat{\Phi}(\omega) \leq C_2(1 + |\omega|_2^2)^{-\tau} \quad \text{for all } \omega \in \mathbb{R}^d, \quad (4)$$

and two positive constants C_1 and C_2 . This setup allows us to use the Matérn kernel, which reproduces Sobolev spaces $H^\tau(\mathbb{R}^d)$, defined as:

$$\Phi_\tau(\cdot, x_j) = C_\tau \|\cdot - x_j\|^{m-d/2} K_{\tau-d/2}(\|\cdot - x_j\|), \quad (5)$$

where K_ν is the modified Bessel function of the second kind and $C_\tau = 2^{1-(\tau-d/2)}/\Gamma(\tau-d/2)$ normalizes the kernel.

Let $X = \{x_1, x_2, \dots, x_{N_X}\} \subset \Omega \cup \partial\Omega$ be a sufficiently dense discrete set (with respect to Ω , Φ , and \mathcal{L}) of N_X trial centers. We seek numerical solutions in finite-dimensional trial spaces spanned by translations of Φ :

$$U_{\Phi, X} := \text{span} \{\Phi(\cdot, x_j) : x_j \in X\} \subset H^\tau(\Omega). \quad (6)$$

The *variational least-squares solution* in the referenced work is defined by

$$u_{VLS}^h := \frac{1}{2} \arg \inf_{v \in U_{\Phi, X}} \left(\|\mathcal{L}v - f\|_{L^2(\Omega)}^2 + h^{-3} \|v - g\|_{L^2(\partial\Omega)}^2 \right), \quad (7)$$

whose error estimates were made in terms of the fill distance of X :

$$h = h_X := \sup_{\zeta \in \Omega} \min_{x_j \in X} \|\zeta - x_j\|_{\ell^2(\mathbb{R}^d)}. \quad (8)$$

In later theorems, fill distances of other sets of points will be denoted with different subscripts. We also need the separation distance of X given by

$$q_X := \frac{1}{2} \min_{\substack{x_i, x_j \in X \\ x_i \neq x_j}} \|x_i - x_j\|_{\ell^2(\mathbb{R}^d)},$$

and the mesh ratio is $\rho_X := h/q_X$.

Since $u_{VLS}^h \in U_{\Phi, X}$, there exist coefficients $\{c_j\} \subset \mathbb{R}^{N_X}$ such that

$$u_{VLS}^h(x) = \sum_{j=1}^{N_X} c_j \Phi(x, x_j).$$

Therefore, the optimization problem (7) can be recast in terms of these coefficients as

$$u_{VLS}^h := \frac{1}{2} \arg \inf_{\{c_j\} \subset \mathbb{R}^{N_X}} \left\{ \int_{\Omega} \left(\sum_{j=1}^{N_X} c_j \mathcal{L}\Phi(x, x_j) - f \right)^2 dx \right. \quad (9) \\ \left. + h^{-3} \int_{\partial\Omega} \left(\sum_{j=1}^{N_X} c_j \Phi(x, x_j) - g \right)^2 dx \right\},$$

whose minimizer $\alpha := [c_1, \dots, c_{N_X}]^T$ is the solution of the following $N_X \times N_X$ matrix system

$$\int_{\Omega} \mathcal{L}\Phi(x, x_l) \left(\sum_{j=1}^{N_X} c_j \mathcal{L}\Phi(x, x_j) - f(x) \right) dx \quad (10) \\ + h^{-3} \int_{\partial\Omega} \Phi(x, x_l) \left(\sum_{j=1}^{N_X} c_j \Phi(x, x_j) - g(x) \right) dx = 0,$$

for $1 \leq l \leq N_X$. Upon proving the stability inequality (2) (i.e., Lemma 3.8 of the referenced work) in the next section, we will have a theoretically sound error estimate for u_{VLS}^h (by Theorem 3.12 and Corollary 3.16 of the referenced work):

Theorem 1. *Let $d \leq 3$ and $\tau \geq k \geq 4$ (hence, $\tau > d/2$). Suppose $\Omega \subset \mathbb{R}^d$ is a bounded domain with C^k -boundary $\partial\Omega$ satisfying an interior cone condition. Let \mathcal{L} in the PDE (1) be a second-order strongly elliptic operator satisfying*

boundary regularity estimates in the form of (3). Also, suppose that the solution $u \in H^k(\Omega)$ to (1) has smoothness order k . Let $\Phi : \Omega \times \Omega \rightarrow \mathbb{R}$ be a symmetric positive definite kernel that reproduces the Sobolev space $H^\tau(\Omega)$ with smoothness τ . Let $u_{VLS}^h \in U_{\Phi, X} \subset H^\tau(\Omega)$, which belongs to the trial space (6) with quasi-uniform trial centers in X and fill distance h , denote the variational least-squares solution defined in (7). Then, the 2-norm condition number of the linear matrix system (10) associated with (7) is bounded above by $Ch^{-4\tau}$. Moreover, the following error estimate holds:

$$\|u - u_{VLS}^h\|_{H^t(\Omega)} \leq Ch^{k-t} \|u\|_{H^k(\Omega)} \quad \text{for any } 0 \leq t \leq k,$$

where C is a generic constant independent of u and u_{VLS}^h .

Theorem 1 suggests that setting $\tau = k$ has no effect on the error estimate but yields the lowest bound on the condition number. In practice, one usually chooses τ based on certain numerical considerations, under the assumption that the solution is at least as smooth as the kernel. In other words, we use $k = \tau$ in theory, even though the true solution smoothness could be greater than τ .

A general framework for proving high-order convergence can be found in [5]. We outline the key elements in the proof for discussions in later sections. In our context, the PDE (1) and numerical methods satisfy the followings:

- **Well-posedness** of the PDE in the sense that any PDE solution can be bounded above by that of the associated data functions under some appropriate norms. The boundary regularity (3) serves this purpose.
- **Trial space** is a finite-dimensional space from which we seek a numerical approximation to the PDE solution. The assumptions made about the regularity/smoothness of the PDE solution determine the choice of the trial space.
- **Stability estimate** bounds all trial functions from above using a data norm (which can be easily computed and may be either continuous or discrete), usually derived from the well-posedness inequality. Its main role is to bound the numerical solution via optimization. Specifically, the objective function in the definition (7) of VLS solutions is essentially (constant multiple of) the right-hand side of the stability inequality. This is typically the most challenging part of designing a convergent numerical method. For instance, the desired stability inequality (2)

uses L^2 -norms on the right-hand side, unlike the Sobolev norms in the boundary regularity. In the referenced work, a Bernstein-type inverse inequality

$$\|u\|_{H^{3/2}(\partial\Omega)} \stackrel{?}{\leq} Ch^{-3/2}\|u\|_{L^2(\partial\Omega)} \quad \text{for all } u \in U_{\Phi, X} \quad (11)$$

is used to derive stability inequality (2) from boundary regularity (3).

We emphasize by using $\stackrel{?}{\leq}$ that this is just a conjectured inequality, which lacks theoretical support due to the mismatch between trial centers $X \in \Omega$ and norms on $\partial\Omega$.

- **Consistency estimates** use the approximation power of the trial space to determine the error bounds and convergence rates of the numerical method. Since the numerical solution is defined via an optimization problem, we can replace the numerical solution in the objective function with some comparison trial function in the error analysis. This comparison function could be, for instance, the interpolant of the true solution from the trial space, which provides an upper bound. The remainder of the analysis can be conducted using standard approximation theory. Interested readers are encouraged to refer to the earlier works cited in the introduction for detailed proofs of convergence. The stability estimates provided in this paper are independent of the consistency analysis.

Evaluating the integrals in the matrix system (10) exactly can be a challenging task due to the complexity of the involved functions and the potential high-dimensionality of the irregularly-shaped domain. To convert the matrix system in (10) into a computable scheme, we use sets of *quadrature nodes* in the domain and on the boundary

$$Y = \{y_1, y_2, \dots, y_{N_Y}\} \subset \Omega \cup \partial\Omega \quad \text{and} \quad Z = \{z_1, z_2, \dots, z_{N_Z}\} \subset \partial\Omega, \quad (12)$$

with positive *quadrature weights*, which are stored in a diagonal matrix for convenience,

$$W = \text{Diag} [\omega_1, \omega_2, \dots, \omega_{N_Y}, \omega_{N_Y+1}, \dots, \omega_{N_Y+N_Z}] \quad (13)$$

to approximate the integrals in Ω and on $\partial\Omega$. Then, an approximate version

of the matrix system (10) can be written as

$$\begin{bmatrix} [\mathcal{L}\Phi](Y, X) \\ h^{-\frac{3}{2}}[\Phi](Z, X) \end{bmatrix}^T W \begin{bmatrix} [\mathcal{L}\Phi](Y, X) \\ h^{-\frac{3}{2}}[\Phi](Z, X) \end{bmatrix} \alpha = \begin{bmatrix} [\mathcal{L}\Phi](Y, X) \\ h^{-\frac{3}{2}}[\Phi](Z, X) \end{bmatrix}^T W \begin{bmatrix} f(Y) \\ h^{-\frac{3}{2}}g(Z) \end{bmatrix}, \quad (14)$$

which is nothing but the least-squares solution to the following $(N_Y + N_Z) \times N_X$ overdetermined matrix system for an unknown coefficient vector $\alpha \in \mathbb{R}^{N_X}$:

$$W^{1/2} \begin{bmatrix} [\mathcal{L}\Phi](Y, X) \\ \vartheta[\Phi](Z, X) \end{bmatrix} \alpha = W^{1/2} \begin{bmatrix} f(Y) \\ \vartheta g(Z) \end{bmatrix}, \quad \text{with } \vartheta = h^{-\frac{3}{2}}. \quad (15)$$

If all data points have fill distances of the same magnitude and the quadrature weights are constant, i.e., $W = \text{Vol}(\Omega)N_Y^{-1}I$, say in the case of Monte Carlo integration, then (15) is exactly the kernel-based least-squares collocation (LSC) systems with oversampling in our prior work [6]. This close proximity motivates proving (2) by the stability inequality in the discrete counterpart.

3. Proof of stability estimates

The theoretical work presented below makes use of our previously established theories on least-squares collocation solutions to (1) from our prior work [6] to prove the target stability inequality (2). We now let the points in the sets (12) play the role of collocation points. Furthermore, we also define the discrete norm for a function u with the set P of N_P points by

$$\|u\|_P^2 := \|u(P)\|_{\ell^2(\mathbb{R}^{N_P})}^2 = \sum_{p_i \in P} |u(p_i)|^2. \quad (16)$$

Then, we can use Y and Z to define discrete norms. For completeness, the *least-squares collocation* solution ([6, Theorem 2.6] with $\theta = 2$ and $\nu = q + 2$) is defined as

$$u_{LSC}^h := \frac{1}{2} \arg \inf_{v \in U_{\Phi, X}} \left(\|\mathcal{L}v - f\|_Y^2 + h_Y^{-d+2q} h_Z^{d-4-2q} \|v - g\|_Z^2 \right), \quad (17)$$

whose objective function stems from the following stability estimate involving discrete norms ([6, Lemma 3.3] with $\nu = q + 2$):

Proposition 1. *Under the assumptions of Theorem 1, for any sets of collocation points $Y \subset \Omega \cup \partial\Omega$ and $Z \subset \partial\Omega$ satisfying the denseness requirement*

$$C (h_Y^{\tau-q-2} + h_Z^{\tau-q-2}) h^{-\tau+q+2} < \frac{1}{2}, \quad (18)$$

the stability inequality

$$\|u^h\|_{H^{q+2}(\Omega)}^2 \leq C \left(h_Y^{d-2q} \|\mathcal{L}u^h\|_Y^2 + h_Z^{d-4-2q} \|u^h\|_Z^2 \right), \quad 0 \leq q \leq \tau - 2, \quad (19)$$

holds for all trial functions $u^h \in U_{\Phi, X} \subset H^\tau(\Omega)$, with some constant C that only depends on q , Ω , Φ and \mathcal{L} .

To prove the discrete stability estimate in (19), we require theoretical tools such as sampling inequalities [10] and inverse inequalities. These inequalities, which differ from the conjecture (11), were proven in our prior work. We direct interested readers to the original articles for more details. It is easy to verify that the collocation matrix in this context corresponds to the overdetermined system in the form of (15) with unity quadrature weight. The trial function that minimizes (17) has expansion coefficients $\{c_j\} \subset \mathbb{R}^{N_X}$ that solve (15) in the least-squares sense, and (14) is the associated normal equation.

Now, we rewrite the inequality (19) as

$$C^{-1} \|u^h\|_{H^{q+2}(\Omega)}^2 \leq h_Y^{-2q} h_Y^d \|\mathcal{L}u^h\|_Y^2 + h_Z^{-2q} h_Z^{-3} h_Z^{d-1} \|u^h\|_Z^2,$$

which matches the form of our targeted inequality in (2). Note that (2) can be proven if, for any given trial function u^h , we can select sets Y and Z so that

$$h_Y^d \|\mathcal{L}u^h\|_Y^2 \leq \|\mathcal{L}u^h\|_{L^2(\Omega)}^2, \quad \text{and} \quad h_Z^{d-1} \|u^h\|_Z^2 \leq \|u^h\|_{L^2(\partial\Omega)}^2 \quad (20)$$

hold, and at the same time, subject to a constraint on fill distances

$$h_Y, h_Z = \mathcal{O}(h)$$

to allow factoring the term h^{2q} to the left-hand side. We present two lemmas to prove (20) before the formal proof of the stability inequality (2).

Lemma 1. *Let $\Omega \subset \mathbb{R}^d$ be a compact domain. Let $v : \Omega \rightarrow \mathbb{R}$ be any Riemann square-integrable function. For any given $C > 0$ and $h > 0$, there exists a discrete set of points $P \subset \bar{\Omega}$ with fill distance $\frac{1}{2}Ch \leq h_P \leq Ch$ satisfying $h_P^d \|v\|_P^2 \leq \|v\|_{L^2(\Omega)}^2$.*

Proof. We present a constructive proof by first picking a sufficiently large rectangular domain $\mathcal{R} := [-l, l]^d \supset \Omega$ with some $l \in \delta\mathbb{N} := d^{-1/2}Ch\mathbb{N}$. Then,

\mathcal{R} can be partitioned by equally sized square subdomains with volume δ^d ; we call this partition \mathcal{P} . We pick an initial set of (possibly non-distinct) points $Q \subset \mathcal{R}$ that can achieve the lower Riemann sum $\underline{R}_{\mathcal{P}}$ on \mathcal{P} . That is,

$$\underline{R}_{\mathcal{P}}(\chi_{\Omega}v^2) = h_Q^d \|v\|_Q^2 \leq \int_{\mathcal{R}} \chi_{\Omega}v^2 dx = \int_{\Omega} v^2 dx = \|v\|_{L^2(\Omega)}^2,$$

where χ_{Ω} is the characteristic function for Ω . Note that the points in Q may not be distinct or even in the domain; we define the set of distinct points $P = \text{unique}(Q \cap \bar{\Omega})$ by removing points outside of $\bar{\Omega}$ and duplicates in Q . By doing so, we must have $h_P = h_Q$ and $\|v\|_P^2 \leq \|v\|_Q^2$.

We conclude the proof by observing two critical scenarios. The first scenario arises when the largest possible fill distance of $P \subset \bar{\Omega} \subset \mathbb{R}^2$ (\mathbb{R}^3) occurs. This happens in a local region where two of the four (eight) points in a 4-square quadrant (8-cube cuboid) region are located in opposite corners. This is illustrated in Figure 1. In general, we have $(2h_P)^2 \leq d(2\delta)^2$ for dimension d . In the second scenario, the smallest fill distance, $d\delta^2 \leq (2h_P)^2$, occurs when all data points are situated at the center of their respective squares (cubes). Therefore, it follows that $\frac{1}{4}C^2h^2 \leq h_P^2 \leq C^2h^2$ as required. \square

In the course of our study, it has come to our attention that similar themes and theoretical results have been explored in an unpublished work [11]. Specifically, the norm equivalency there were built upon/for nested quasiuniform points generated by a geometrically greedy algorithm [12].

Lemma 2. *Let $\partial\Omega \subset \mathbb{R}^d$ be a codimension-1, C^1 -smooth, connected and compact manifold. Let $v : \partial\Omega \rightarrow \mathbb{R}$ be any Riemann square-integrable function. Denote by $r_{\partial\Omega} > 0$ a constant dependent on $\partial\Omega$ for which the constant-along-normal extension is well-defined in the narrow band domain of radius $r < r_{\partial\Omega}$. For any given $C > 0$ and $h > 0$ sufficiently small with respect to $r_{\partial\Omega}$ and other generic constants, there exists a discrete set of points $P \subset \partial\Omega$ with fill distance $\frac{1}{2}Ch \leq h_P \leq Ch$ satisfying $h_P^{d-1} \|v\|_P^2 \leq \|v\|_{L^2(\partial\Omega)}^2$.*

Proof. We prove this boundary version by embedding and application of Lemma 1. First, we pick a constant $r < r_{\partial\Omega}$ so that the Euclidean closest point function

$$\text{ecp}(x) := \arg \min_{y \in \partial\Omega} |x - y| \quad \text{for } x \in B(\partial\Omega)$$

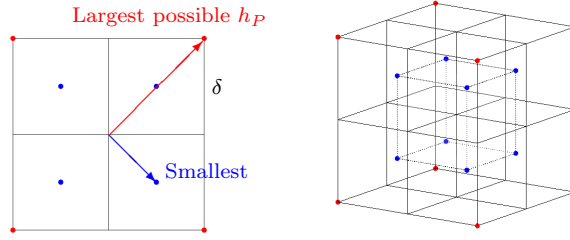


Figure 1: An illustration of the distribution of data points contributing to the lower Riemann sum based on a partition with equally sized subdomains with edge length δ . The red points showcase a distribution that maximizes the fill distance when some points are located at opposite corners of one quadrant/cuboid region. The blue points show a distribution that minimizes the fill distance when all the points are in the centers of all quadrant/cuboid regions.

is C^0 -continuous in the r -narrow band domain:

$$B(\partial\Omega) := \{x \in \mathbb{R}^d : \|x - y\|_2 \leq r < r_{\partial\Omega}, \quad \text{for some } y \in \partial\Omega\}.$$

This is a relaxed version of the ecp-Calculus in [13] as we do not require any differentiability in this proof. Using [14, Lemma 3.1] to relate the norms of surface functions and their constant-along-normal extensions defined by $x := y + t\vec{n}(y) : \partial\Omega \rightarrow \Gamma_t$ for $y \in \partial\Omega$ and $t \in [0, r]$, there exists a constant $C_{\partial\Omega}$ that depends only on $\partial\Omega$ such that

$$\|v \circ \text{ecp}\|_{L^2(B(\partial\Omega))}^2 := \int_{-r}^r \|v \circ \text{ecp}\|_{L^2(\Gamma_t)}^2 dt \leq C_{\partial\Omega} r \|v\|_{L^2(\partial\Omega)}^2 \quad (21)$$

holds for all $v \in L^2(\partial\Omega)$.

For any sufficiently small h , let us focus on some rectangular region \mathcal{R} containing the band $B(\partial\Omega)$. We partition \mathcal{R} as in the previous proof with $r = C^d h / (2^d C_{\partial\Omega}) < r_{\partial\Omega}$. Now, we apply Lemma 1 with the given constants $C, h > 0$ to the constant-along-normal extension $v \circ \text{ecp} : B(\partial\Omega) \rightarrow \mathbb{R}$ of any given $v \in L^2(\partial\Omega)$. By (21), this gives us an initial set of distinct points $Q \subset B(\partial\Omega)$ so that

$$\begin{aligned} h_Q^d \|v \circ \text{ecp}\|_Q^2 &\leq \|v \circ \text{ecp}\|_{L^2(B(\partial\Omega))}^2 \\ &\leq C_{\partial\Omega} r \|v\|_{L^2(\partial\Omega)}^2 \\ &= \frac{C^d}{2^d} h \|v\|_{L^2(\partial\Omega)}^2. \end{aligned} \quad (22)$$

We define the desired boundary point set as $P = \text{unique}(\text{ecp}(Q)) \subset \partial\Omega$. Its fill distance h_P is defined similarly to (8), but the supremum is taken over a smaller set, $\partial\Omega$. Consequently, we must have $h_P \leq h_Q$. From the previous proof, we understand that the minimum fill distance occurs only for certain point distributions. Any alteration in the points will result in a change from this minimum fill distance. Based on these observations, we conclude that the fill distance h_P can only assume values within the range of h_Q . In particular, from Lemma 1, we know that the range of possible fill distance is $\frac{1}{2}Ch \leq h_P \leq h_Q \leq Ch$. Continuing to work on (22) yields the following results:

$$\begin{aligned} \|v\|_{L^2(\partial\Omega)}^2 &\geq \frac{1}{h} \left(\frac{2}{C} h_P \right)^d \|v \circ \text{ecp}\|_Q^2 \\ &\geq h^{d-1} \|v \circ \text{ecp}\|_P^2 \\ &= h^{d-1} \|v\|_P^2, \end{aligned} \tag{23}$$

and the proof is completed. \square

Remark 1

In the proof in Lemma 2, the fill distance h_P is implicitly characterized by Euclidean distances. For sufficiently small $h < r_{\partial\Omega}$, then we can pick a narrow band domain to have radius $r < h$. From the proof of our earlier work [15, Lemma 3.2], we know the two fill distances are equivalent, i.e., $C_1 h_P \leq h_{P,\partial\Omega} \leq C_2 h_P$ holds for some C_1, C_2 depending on the diameter of $\partial\Omega$. Using $h_{P,\partial\Omega}$ in Lemma 2 only influences the generic constants in the proof, as the geodesic fill distance $h_{P,\partial\Omega}$ is proportional to h_P . \square

Through Lemmas 1 and 2, we have confirmed the existence of sets Y and Z that satisfy the conditions of (20) and the fill distance constraints $h_Y, h_Z = \mathcal{O}(h)$. With these conditions met, we can now apply these findings to establish the stability inequality (2) of the main theorem.

Theorem 2. *Under the assumptions of Theorem 1, the stability inequality in (2)*

$$C^{-1} h^{2q} \|u^h\|_{H^{q+2}(\Omega)}^2 \leq \|\mathcal{L}u^h\|_{L^2(\Omega)}^2 + h^{-3} \|u^h\|_{L^2(\partial\Omega)}^2, \quad 0 \leq q \leq \tau - 2,$$

holds for all trial functions $u^h \in U_{\Phi,X} \subset H^\tau(\Omega)$ that are Riemann square-integrable with some constant C that only depends on q, Ω, Φ and \mathcal{L} .

Proof. We denote C_{18} as the generic constant in (18), with its exact value being non-essential for this proof. We apply Lemma 1 and Lemma 2 with $C = (5C_{18})^{-1/(\tau-q-2)}$. This enables us to select sets of collocation points $Y \subset \overline{\Omega}$ and $Z \subset \partial\Omega$ that satisfy the denseness requirement (18). Consequently, this ensures that the discrete stability estimate (19) holds. These sets Y and Z also meet the condition that $h_Y = \mathcal{O}(h) = h_Z$, which can be used to provide lower estimate to L^2 -norms in (20). Thus, the proof is complete. \square

Note that we simply adopt the theory for LSC method to prove Theorem 2, which does not contain any denseness requirement as there are no collocation or quadrature points in the statement.

4. Implications to least-squares collocation methods

Before we move on, let's clarify some potential confusion around the different "weights" used in our context so far. The "quadrature weights" are the coefficients applied to function evaluations at quadrature points to approximate integrals. In our prior work, we also called the LSC solutions in (17) "weighted least-squares" solutions. In this context, "weighted" refers to the fill distances-related boundary scaling factor $\vartheta = (h_Y^{-d+2q} h_Z^{d-4-2q})^{1/2}$ inside the objective function, which serves to balance the scale differences between the differential operator and boundary conditions. Finally, the "weight matrix" in the WLS solutions (29), which is defined later in page 18, refers to the matrix that is multiplied with the overdetermined system. This system already includes the theoretical scaling factor. This multiplication is done prior to solving the system using a least-squares approach.

We will now summarize by comparing the VLS solutions (7) and the LSC solutions (17). This comparison reveals that each approach has its pros and cons:

- The VLS solutions provide broader convergence estimates, ranging from L^2 to H^τ . In contrast, the LSC solutions offer estimates from $H^{\lceil d/2 \rceil}$ to H^τ , which translate to H^2 -convergence in dimensions $d \leq 3$, c.f. assumption in Theorem 1. We observe similar numerical performance as reported in [6], where the L^2 errors show two additional orders of convergence compared to the H^2 errors.

- The VLS solutions require integrations, and its convergence proofs do not account for quadrature error. The exponentially decaying local Lagrange functions [16] (applicable to the Matérn kernel and more) are efficient tools for evaluating boundary integrals. Conversely, the LSC solutions do not involve integration and are thus free from quadrature error.
- The approximation to VLS solutions imposes no restrictions on quadrature nodes except for accuracy concern. However, the collocation points in the LSC solutions must satisfy the trial center-dependent denseness requirement (18). Locally refining collocation points, without an appropriate weight matrix, often does not improve the accuracy of collocation solutions.
- In terms of the weight matrix W in approximating (15), the VLS solutions naturally employ quadrature weights to define a data point-dependent matrix for the WLS. The theory in [6] regarding the LSC solutions does not permit the additional term W , which could pose accuracy issues when dealing with collocation points with a large mesh ratio. In the second half of this paper, we prove that this concern is unfounded.

Our next goal is to establish another weighted-discrete stability estimate by finding an additional upper bound for the proven stability inequality in (2). This would lead to a numerical scheme where the associated numerical solution is defined by the weighted least-squares formulation in (15). Ideally, the conditions on the weight matrix could accommodate easy-to-compute alternatives beyond merely quadrature weights. This is particularly relevant given the difficulty of determining quadrature weights on irregular domains in higher dimensions. However, the challenge lies in ensuring that any fixed discrete overestimate to an integral holds for all possible trial functions.

4.1. A uniform bound for $L^2(\Omega)$ -norm in the trial space

Here is a quick recap of what is discussed in [17, Theorem 15] for continuous and symmetric positive definite kernel K on a compact set Ω . Mercer's theorem ensures the existence of eigenvalues $\lambda_1 \geq \lambda_2 \geq \dots > 0$ with a decay rate

$$\sqrt{\lambda_{j+1}} < Cj^{-\tau/d},$$

where C is only dependent on K and Ω , and the eigenfunctions ϕ_j that are orthonormal in $L^2(\Omega)$ and orthogonal in its native space $\mathcal{N}(\Omega)$ with $\|\phi_j\|_{\mathcal{N}(\Omega)} = \lambda_j^{-1}$ for any j [17, Theorem 2] such that

$$K(x, y) = \sum_{j=1}^{\infty} \lambda_j \phi_j(x) \phi_j(y) \quad x, y \in \Omega. \quad (24)$$

Let $u \in U_{K,X}$ be defined as in (6) with K in place of kernel Φ . By definition of $U_{K,X}$, express u as a linear combination of the kernel $K(\cdot, x_i)$ centered at $x_i \in X$, i.e.,

$$u(x) = \sum_{i=1}^{N_X} a_i K(x, x_i)$$

for some coefficients a_i . We introduce coefficients $b_j = \sum_{i=1}^{N_X} a_i \phi_j(x_i)$ to simplify this expression for u :

$$u(x) = \sum_{j=1}^{\infty} b_j \lambda_j \phi_j(x).$$

Next, we compute the L^2 -norm square of u . Using the orthonormality of the ϕ_j , this is given as

$$\|u\|_{L^2(\Omega)}^2 = \int_{\Omega} |u(x)|^2 dx = \sum_{j=1}^{\infty} b_j^2 \lambda_j^2 = b^T \underbrace{[\text{diag}(\lambda_1^2, \lambda_2^2, \dots)]}_{=: D_{\lambda}} b, \quad (25)$$

where $b = [b_1, b_2, \dots]^T$ is the u -dependent coefficient vector with respect to eigenfunctions.

On the quadrature side, for nodes in $y_k \in Y$ with positive quadrature weights in $\omega_k \in W$ for $k = 1, \dots, N_Y$, we expand the nodal values of u in the quadrature formula using Mercer's expansion as follows

$$\begin{aligned} \sum_{k=1}^{N_Y} \omega_k |u(y_k)|^2 &= \sum_{k=1}^{N_Y} \omega_k \left(\sum_{j=1}^{\infty} b_j \lambda_j \phi_j(y_k) \right)^2 \\ &= \sum_{j=1}^{\infty} \sum_{l=1}^{\infty} b_j b_l \left(\sum_{k=1}^{N_Y} \omega_k \lambda_j \phi_j(y_k) \lambda_l \phi_l(y_k) \right) = b^T G b. \end{aligned} \quad (26)$$

The jl -entries of the matrix G were defined by:

$$[G]_{jl} = \sum_{k=1}^{N_Y} \omega_k \lambda_j \phi_j(y_k) \lambda_l \phi_l(y_k), \quad (27)$$

which is a Gram matrix and must be semi-positive definite.

The following theorem is crucial for understanding the role of norm equivalency in implementing the necessary numerical integration to find u_{VLS}^h . It leads to a conclusion that high-order quadrature rules are not essential to match the convergence order of the kernel method.

Theorem 3. *Let K be a continuous and positive definite kernel on a compact set Ω . Define a finite-dimensional trial space $U_{K,X}$ of K on some set of trial centers $X \subset \Omega$. Then, for any sufficiently dense set, with respect to K and Ω but not X , of quasi-uniform points $P = \{p_1, \dots, p_N\} \subset \Omega$, there exists a set of zeroth-order quadrature weights, $\{\tilde{\omega}_1, \dots, \tilde{\omega}_{N_P}\} \in \tilde{W}$, that are not connected to any convergent quadrature rule but still can be used to under- and overestimate the $L^2(\Omega)$ -norm of all trial functions. That is, the following inequality holds:*

$$\frac{1}{4} \|u\|_{P, \tilde{W}}^2 \leq \|u\|_{L^2(\Omega)}^2 \leq 4 \|u\|_{P, \tilde{W}}^2 := 4 \sum_{k=1}^N \tilde{\omega}_k |u(p_k)|^2 \quad \text{for all } u \in U_{K,X}.$$

Proof. This inequality can be reformulated in terms of coefficients b using equations (25) and (26) as

$$\frac{1}{4} b^T \tilde{G} b \leq b^T D_\lambda b \leq 4 b^T \tilde{G} b \quad \text{for all } b,$$

where \tilde{G} is the Gram matrix associated with some yet-to-be-determined zeroth-order quadrature weights \tilde{W} . We first note that each element G_{jl} of the matrix G is obtained by summing the products of quadrature weights ω_k and the corresponding function values, over all quadrature points $p_k \in P$. This sum forms an approximation to the integral over Ω . Given the orthogonality of eigenfunctions, the matrix G tends towards D_λ as $h_P \rightarrow 0$ (or $N_P \rightarrow \infty$, provided P is quasi-uniformly refined, i.e., $h_P \leq CN_P^{-1/d}$), and W represents any quadrature weights linked to a convergent quadrature rule. This limit argument is independent of X . The class of integrands under current consideration that are smooth, decay with respect to indices

j, l , and have a bounded $H^\tau(\Omega)$ -norm, i.e., $\|\lambda_j \phi_j\|_{\mathcal{N}(\Omega)} \leq 1$. Thus, we can select a large enough N_P such that G is close to D_λ . Here, closeness is defined such that the j -th eigenvalue of G , $\lambda_j(G)$, lies within the interval $[\frac{1}{2}\lambda_j(D_\lambda), 2\lambda_j(D_\lambda)]$.

We now perform a second perturbation of G by altering quadrature weights W to some nearby values \widetilde{W} , resulting in a new Gram matrix \widetilde{G} . We keep the perturbation small so that this new matrix has the property that its j -th eigenvalue, denoted as $\lambda_j(\widetilde{G})$, lies within $[\frac{1}{2}\lambda_j(G), 2\lambda_j(G)]$ or $[\frac{1}{4}\lambda_j(D_\lambda), 4\lambda_j(D_\lambda)]$. By considering any basis formed by the eigenvectors of \widetilde{G} , we show that

$$\frac{1}{4}b^T D_\lambda b \leq b^T \widetilde{G} b \leq 4b^T D_\lambda b \quad \text{for all } b.$$

Given the symmetry of this inequality, one can reverse the roles of $b^T D_\lambda b$ and $b^T \widetilde{G} b$ and our claim is proven. \square

Remark 2

The above analysis is applicable to a wider class of symmetric positive definite kernels. However, to align with the convergence proof in other sections, we primarily focus on kernels that reproduce Sobolev spaces, such as the Matérn kernels Φ of smoothness order $\tau > d/2$, whose native space is $H^\tau(\Omega)$. Moreover, it is also applicable to the restricted Matérn kernels $\Phi|_{\partial\Omega \times \partial\Omega}$ on the boundary [18], whose native space is $H^{\tau-1/2}(\partial\Omega)$. \square

4.2. Weighted-LS kernel-based collocation method is convergent

Our final theoretical goal is to demonstrate that the VLS solver can be implemented without using exact quadrature weights, which becomes a WLS problem. In this section, we walk the reader through the main ideas of the construction of a convergent method for the WLS solutions in (15). Using the weight-discrete norm defined in Theorem 3, our goal is to establish another stability estimate involving weighted-discrete norms:

$$C^{-1}h^{2q}\|u^h\|_{H^{q+2}(\Omega)}^2 \leq \|\mathcal{L}u^h\|_{Y, \widetilde{W}_Y}^2 + h^{-3}\|u^h\|_{Z, \widetilde{W}_Z}^2 \quad \text{for all } u^h \in U_{\Phi, X}, \quad (28)$$

which can be proven by overestimation of (2). This inequality holds for some zeroth-order weights $\widetilde{W}_Y, \widetilde{W}_Z$. The solution to the associated kernel-based

weighted least-squares collocation method is defined as

$$u_{WLS}^h := \frac{1}{2} \arg \inf_{v \in U_{\Phi, X}} \left(\|\mathcal{L}v - f\|_{Y, \widetilde{W}_Y}^2 + h^{-3} \|v - g\|_{Z, \widetilde{W}_Z}^2 \right), \quad (29)$$

that requires solving the resultant overdetermined system (15) in the least-squares sense.

As remarked in the previous section, Theorem 3 has already demonstrated that the continuous and weighted-discrete norms on the boundary are equivalent in the trial space

$$\|u^h\|_{L^2(\partial\Omega)}^2 \sim \|u^h\|_{Z, \widetilde{W}_Z}^2 \quad \text{for all } u^h \in U_{\Phi, X}, \quad (30)$$

using constants $\frac{1}{4}$ and 4 in this norm equivalency.

Our remaining task is to handle the norms of $\mathcal{L}u^h \in H^{\tau-2}(\Omega)$ for any $u^h \in U_{\Phi, X}$. We need another kernel Ψ that satisfies the decay condition (4) with a rate of $\tau - 2$ rather than τ . For instance, if the Matérn kernel is used, we can simply set $\Psi = \Phi_{\tau-2}$ as defined in (5).

The problem is that, in general cases, applying the differential operator \mathcal{L} to $u^h \in U_{\Phi, X}$ results in a function $\mathcal{L}u^h \notin U_{\Phi, X}$ that is not in same trial space. To bound its L^2 -norm using Theorem 3, we might consider some projection or best approximation from $H^{\tau-2}(\Omega)$ to $U_{\Psi, X}$. However, this approach is flawed as the nodal values would change after projection, leading to the disappearance of the desired weighted-discrete norm in the upper bound from the analysis. To circumvent this issue, our solution is to project using a sufficiently dense set of collocation points Y . This denseness is quantitatively defined by the condition:

$$C(h_Y/h)^{\tau-2} < 1/8, \quad (31)$$

and along with that for Theorem 3 to apply and, hence, for the existence of the weight \widetilde{W}_Y for the norm equivalence inequalities to hold. Instead of X , we define the trial space $U_{\Psi, Y} \subset H^{\tau-2}(\Omega)$ on Y . We denote the interpolant of $v \in H^{\tau-2}(\Omega)$ on Y in the trial space $U_{\Psi, Y}$ as $s_v = I_{\Psi, Y}v$.

For the sake of simplicity, we use C to denote all generic constants that appear below, bearing in mind that these may assume different values in different contexts. Using Theorem 3 and an error estimate for kernel inter-

polution [19], we get

$$\begin{aligned}
\|v\|_{L^2(\Omega)}^2 &\leq \|s_v\|_{L^2(\Omega)}^2 + \|v - s_v\|_{L^2(\Omega)}^2 \\
&\leq 4\|s_v\|_{Y, \widetilde{W}_Y}^2 + Ch_Y^{2\tau-4}\|v\|_{H^{\tau-2}(\Omega)}^2 \\
&\leq 4\|v\|_{Y, \widetilde{W}_Y}^2 + Ch_Y^{2\tau-4}\|v\|_{H^{\tau-2}(\Omega)}^2 \quad \text{for all } v \in H^{\tau-2}(\Omega).
\end{aligned}$$

For any $u^h \in U_{\Phi, X} \subset H^\tau(\Omega)$, if we set $v = \mathcal{L}u^h$, we can derive the following inequality

$$\begin{aligned}
\|\mathcal{L}u^h\|_{L^2(\Omega)}^2 &\leq 4\|\mathcal{L}u^h\|_{Y, \widetilde{W}_Y}^2 + Ch_Y^{2\tau-4}\|\mathcal{L}u^h\|_{H^{\tau-2}(\Omega)}^2 \\
&\leq 4\|\mathcal{L}u^h\|_{Y, \widetilde{W}_Y}^2 + Ch_Y^{2\tau-4}\|u^h\|_{H^\tau(\Omega)}^2 \\
&\leq 4\|\mathcal{L}u^h\|_{Y, \widetilde{W}_Y}^2 + Ch_Y^{2\tau-4}h^{-2\tau+4+2q}\|u^h\|_{H^{2+q}(\Omega)}^2,
\end{aligned}$$

which is the result of an inverse inequality found in [6, Lemma 3.2] of our prior work. Now, we can then use this result to bound (2) with generic constant C_2 from the above as follows

$$\begin{aligned}
C_2^{-1}h^{2q}\|u^h\|_{H^{q+2}(\Omega)}^2 &\leq 4\left(\|\mathcal{L}u^h\|_{Y, \widetilde{W}_Y}^2 + h^{-3}\|u^h\|_{Z, \widetilde{W}_Z}^2\right) \\
&\quad + h^{2q}\left(C(h_Y/h)^{\tau-2}\|u^h\|_{H^{2+q}(\Omega)}\right)^2,
\end{aligned}$$

which holds for all $u^h \in U_{\Phi, X}$. Under the denseness requirement (31) by using yet another generic constant C , c.f., the one in (18) for the non-weighted version, the weighted-discrete stability inequality in (28) holds for all $u^h \in U_{\Phi, X}$. Since \widetilde{W} only contains bounded quadrature weights, the L^∞ consistency analysis from our previous work directly applies to the new collocation method (29). We refer readers to [6] for details.

Under the same denseness requirement (31), we can invert the above proof to show the above bounds hold in reverse order:

$$\begin{aligned}
\|v\|_{Y, \widetilde{W}_Y}^2 &\leq \|s_v\|_{Y, \widetilde{W}_Y}^2 \leq 4\|s_v\|_{L^2(\Omega)}^2 \\
&\leq 4\left(\|v\|_{L^2(\Omega)}^2 + \|v - s_v\|_{L^2(\Omega)}^2\right) \\
&\leq 4\left(\|v\|_{L^2(\Omega)}^2 + Ch_Y^{2\tau-4}\|v\|_{H^{\tau-2}(\Omega)}^2\right) \quad \text{for all } v \in H^{\tau-2}(\Omega),
\end{aligned}$$

or, for any $u^h \in U_{\Phi, X} \subset H^\tau(\Omega)$, we have

$$\|\mathcal{L}u^h\|_{Y, \widetilde{W}_Y}^2 \leq 4\|\mathcal{L}u^h\|_{L^2(\Omega)}^2 + 4Ch_Y^{2\tau-4}h^{-2\tau+4+2q}\|u^h\|_{H^{2+q}(\Omega)}^2.$$

When coupled with the boundary counterpart in (30), we can use the zeroth-order quadrature weights \widetilde{W}_Y and \widetilde{W}_Z , whose existence is ensured by Theorem 3, to establish the norm equivalency as follows:

$$\|\mathcal{L}u^h\|_{L^2(\Omega)}^2 + h^{-3}\|u^h\|_{L^2(\partial\Omega)}^2 \sim \|\mathcal{L}u^h\|_{Y,\widetilde{W}_Y}^2 + h^{-3}\|u^h\|_{Z,\widetilde{W}_Z}^2 \quad \text{for all } u^h \in U_{\Phi,X}. \quad (32)$$

With this stronger observation, the convergence of the WLS solutions in (29) can be proven via that of the VLS solutions (7). Consequently, Theorem 1 applies to (29) resulting in the following convergence theorem.

In the following section, we will demonstrate how straightforward strategies for generating zeroth-order quadrature weights can yield promising numerical results.

5. Numerical Examples

While the idea of not using any quadrature weight in a VLS formulation might initially seem counterintuitive, this section aims to provide both theoretical arguments and numerical results demonstrating that such an approach is indeed feasible in our considered kernel-based collocation setting. This becomes particularly handy when considering the challenges associated with finding weights in higher dimensions and dealing with scattered data.

For the sets of data points X , Y , and Z specified in each numerical example, let us detail all tested methods in terms of the linear system as shown in (15). All methods use a boundary scaling factor $\vartheta = h^{-\frac{3}{2}}$ and are defined as follows:

VLS-Tp: Approximation to the variational least-squares solution (7), with integrals approximated by quadrature weights W using the Trapezoidal rule.

WLS-Id: Weighted least-squares solution (29), obtained by solving the system in (15) with a constant weight $W = I$.

WLS-Rd: This method is a counterpart to WLS-Id but uses a random weight W where $\text{Diag}(W)$ is distributed uniformly in the range $[0.5, 1.5]$.

If the constant and random W , as zeroth-order quadrature weights, could uphold the equivalency in (32), then VLS-Tp and the two WLS solutions should exhibit the same convergence rate. However, they may be dictated by different generic constants. As a result, despite similar convergence rates, the actual accuracy of these methods may vary.

Denote $\alpha_{\mathcal{W}}$ and α_I as the coefficient vectors of the WLS solutions with any positive weights \mathcal{W} and I , respectively. Let us also rewrite the linear system (15) in a simplified form $A\alpha = b$. We then have the following:

$$\begin{aligned} \|\mathcal{W}(A\alpha_{\mathcal{W}} - b)\| &\leq \|\mathcal{W}\| \|A\alpha_{\mathcal{W}} - b\| \\ &\leq \|\mathcal{W}\| \|A\alpha_I - b\| = w_{\max} \|A\alpha_I - b\|. \end{aligned}$$

By reversing the argument, we find that $\|A\alpha_I - b\| \leq w_{\min}^{-1} \|\mathcal{W}(A\alpha_{\mathcal{W}} - b)\|$. If we substitute α_I into the weighted objective function, we get

$$\|\mathcal{W}(A\alpha_I - b)\| \leq w_{\max} \|A\alpha_I - b\| \leq \kappa(\mathcal{W}) \|A\alpha_I - b\|.$$

This suggests that if the condition number $\kappa(\mathcal{W})$ is small, then the WLS-Id solution almost solves the problem with weight \mathcal{W} . Conversely, we also have

$$\|A\alpha_{\mathcal{W}} - b\| \leq w_{\min} \|\mathcal{W}(A\alpha_{\mathcal{W}} - b)\| \leq \kappa(\mathcal{W}) \|\mathcal{W}(A\alpha_{\mathcal{W}} - b)\|.$$

It is important to note that linear algebra manipulations can only address a single linear system at a time. Therefore, they cannot be used to derive a general convergence theory. But, as long as $\kappa(\mathcal{W})$ is moderate, the above calculations show that the WLS-Id solution nearly solves the WLS optimization problem with weights \mathcal{W} , achieving close (but of course, somewhat larger) objective values, and vice versa. This observation suggests that WLS-Id and WLS-Rd always exhibit similar numerical performance, a claim we intend to verify. Additionally, this motivates us to conduct tests on collocation points Y and Z with large mesh ratios, which lead to an increase in the condition numbers of the Trapezoidal weights as N_Y increases.

Example 1 (Observing predicted convergence rates)

For the sake of reproducibility and to provide clear evidence supporting our theories, we focus on simple numerical setups. We consider the domain $\Omega = (-1, 1)^2$ with regular trial centers X , varying the squared number N_X up to 81^2 . Interior collocation points Y are constructed by tensor product grid data, allowing for straightforward calculations to obtain the Trapezoidal weights. Here is the exact procedure: For each oversampling ratio $\gamma \in 1, 1.5, \dots, 4$, we generate an initial regular grid $P \subset \overline{\Omega}$ with $N_Y = \lceil (\gamma N_X)^{1/2} \rceil^2 \approx \gamma N_X$. Then, we apply a coordinate transform $T : \overline{\Omega} \rightarrow \overline{\Omega}$ to P , and set $Y = T(P)$ and $Z = T(P) \cap \partial\Omega$. The fill distances h_Y and h_Z for these transformed points are of the same magnitude. In this

example, we do not consider varying the h_Y/h_Z ratio based on the numerical results from our prior work [6]. In there, the numerical method is WLS with $W = I$ and boundary scaling factors $\vartheta = ((h_Z/h_Y)^{(d/2-q)\theta} h_Z^{-2\theta})^{1/2}$ for all $\theta \geq 0$. Aside from the problem of ill-conditioning, the WLS methods with a full range of scaling factors demonstrated the same H^2 -convergence rate. The effects of using different scaling factors in that context are similar to the effects of varying the h_Y/h_Z ratio in this study. Two test problems were considered:

PDE 1. We consider the modified Helmholtz equation $\Delta u - u = f$ subject to the Dirichlet boundary condition. The exact solution $u^* = \text{sech}(\pi(x - 0.5)) + \text{sech}(\pi(y - 0.75))$ is used to generate PDE data. The sine-transform [20], defined component-wise by $T(P) = \sin(\pi P/2)$, is used in this case.

PDE 2. We examine the Poisson equation $\nabla \cdot (c \nabla u) = f$ with a strictly negative diffusion tensor $c(x, y) = -\arctan(100(x + y)) - 3\pi/4$, subject to the Dirichlet boundary condition. The exact solution is taken to be $u^* = (1 - x^2) \cos(\pi y/2)$. Here, we use the componentwise signed-square transform $T(P) = \text{sgn}(P)P^2$ to define collocation points and collocate the PDE in non-divergence form.

Note that the transformations T selected in PDEs 1 and 2 were chosen for demonstration purposes, and not based on specific information from the PDEs themselves. Figure 2(a)–(b) shows the distributions of $N_Y = 40^2$ sine-transformed and signed-squared collocation points Y for PDEs 1 and 2 respectively. The background color in both subfigures represents the color contour of the PDE source function f .

We use the Matérn kernel (5) with orders $\tau = 4, 5, 6$ and scale $r \leftarrow \epsilon r$ with a shape parameter $\epsilon = 5$ for all τ . Such selections of smoothness order and shape parameters allow us to observe typical behavior in kernel-based collocation methods. We report relative L^2 errors, which are computed using $\ell^2(P)$ -norms of the nodal values of the error (or difference) function and the exact (or reference) solution on a regular point set P consisting of 86^2 points. The convergence profiles for PDE 1 and PDE 2 are shown in Figures 3 and 4, respectively, each containing three subfigures for each kernel smoothness τ . Errors associated with a small oversampling ratio $\gamma \leq 2$ are shown individually, while those with $\gamma \geq 2.5$ are collectively represented in

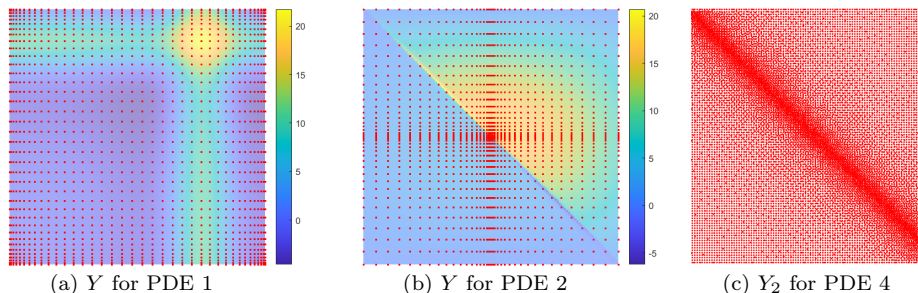


Figure 2: Distribution of $N_Y = 40^2$ sine-transformed (PDE 1), signed-squared (PDE 2), and NodeLab [21] generated (PDE4) collocation points, overlaying the color contour of the corresponding source function f (PDEs 1 and 2).

shaded areas. The predicted convergence rate from Theorem 1 is simply τ , and a reference slope has been added for ease of comparison.

PDE 1 is a relatively easy test problem owing to its smooth and artificial analytic solution. From Figure 3, it is clear that a sufficiently high oversampling ratio is necessary. Most importantly, the two WLS-xx methods and VLS-Tp all converge at the same rate, a result that validates the convergence theory of WLS as discussed in Section 4.2. Notably, the convergence is not impacted by the increasing condition number $\kappa(W)$ of the Trapezoidal weight W , which grows at a rate of $\mathcal{O}(N_Y^3)$ in both coordinate transforms. The accuracy of WLS-Id and WLS-Rd is nearly identical.

Conversely, PDE 2 is more difficult, even with its analytic solution. This is attributed to the source function that changes rapidly along the line $x+y = 0$. The error profiles are not as linear as in PDE 1, yet the trend aligns with the forecasted convergence rate. The accuracy advantage of VLS-Tp over the other two WLS-xx methods is not immediately apparent, but it appears to be more accurate when $\tau = 6$.

Example 2 (Superconvergence with zeroth order quadrature)

Superconvergence in the context of kernel-based interpolation [22] is a complex interplay between the smoothness and the localization of the function. This example aims to replicate similar results within the framework of VLS and WLS methods.

PDE 3. We consider the modified Helmholtz equation $\Delta u - u = f$ subject to the Dirichlet boundary condition. The exact solution is a Gaussian

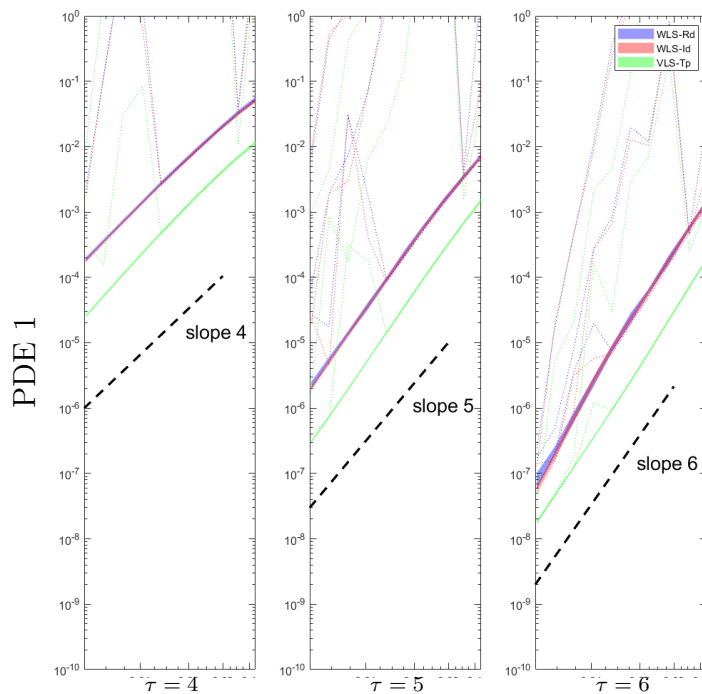


Figure 3: Relative L^2 convergence profiles of VLS-Tp, WLS-Id, and WLS-Rd for PDE 1 using the Matérn kernel with smoothness orders $\tau = 4, 5, 6$. Errors associated with oversampling ratio $\gamma \in \{1.0, 1.5, 2.0\}$ are shown individually, while those with $\gamma \in \{2.5, 3.0, 3.5, 4.0\}$ are collectively represented in a shaded area. The predicted convergence rate from Theorem 1 is represented by the reference slope.

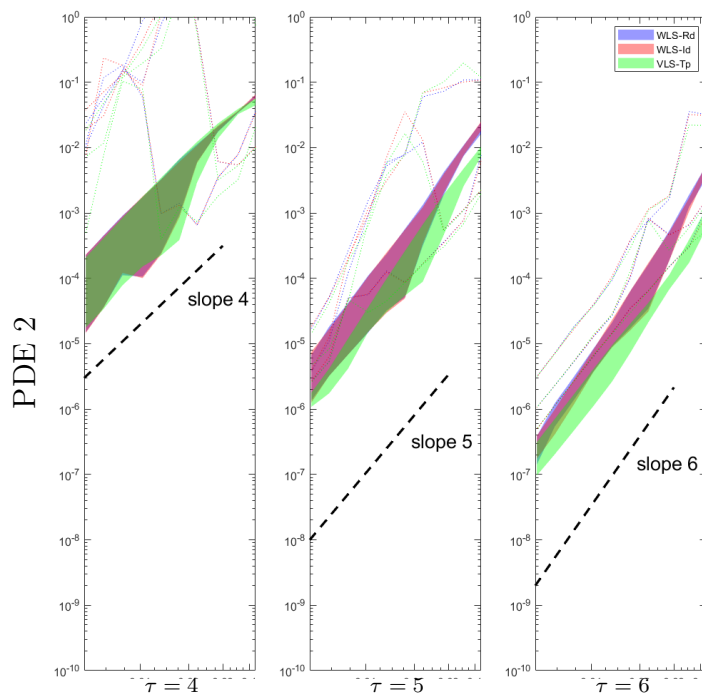


Figure 4: Relative L^2 convergence profiles for PDE 2, presented in the same format as in Figure 3.

function $u^*(x, y) = \exp(-10[(x - x_0)^2 + (y - y_0)^2])$. The signed-square transform is used to increase collocation point density near the origin.

In the first test, we set $[x_0, y_0] = [0, 0]$ which results in a high density of collocation points within the support of the Gaussian. In the second test, we choose $[x_0, y_0] = [0.5, 0.75]$ for a contrary setup with lower point density. The resulting error profiles for both scenarios are displayed in Figures 5 and 6. Figure 5 exhibits high accuracy and clear superconvergence, demonstrating the benefits of having a high-density collocation point set at the right place. On the other hand, Figure 6 shows an even faster convergence rate, but the approximation accuracy compared to Figure 5 is less. This highlights the influence of point density on the balance between convergence rate and approximation accuracy in the VLS and WLS methods. All findings here are consistent with our observations in Example 1, where all methods converged at the same rate.

Example 3 (Collocation in divergence form with nearly singular diffusion tensor)

In this final example, we examine a PDE characterized by a simple data function, but without an exact solution:

PDE 4. We consider the Poisson equation $\nabla \cdot (c \nabla u) = 1$, equipped with a strictly negative diffusion tensor $c(x, y) = -\arctan(100(x + y)) - 3\pi/4$, and subject to the Dirichlet boundary condition $u|_{\partial\Omega} = 0$. Given a set of trial center X , we employ an oversampling ratio $\gamma = 2.5$ to generate regular Y_1 and Z . The NodeLab [21] package is used to produce scattered 7338 data points as Y_2 , densely populating along $x - y = 0$, as illustrated in Figure 2(c). Then, we take $Y = Y_1 \cup Y_2$ as the set of PDE collocation points. The PDE is collocated in divergence form.

In these examples, we only focus on divergence form PDEs because non-divergence form PDEs present considerable challenges for many methods, including both our VLS-Tp (on some tensor grid Y) and WLS-Id methods and also RBF-FD methods. In fact, these methods often fail to solve non-divergence form PDEs correctly.

To validate the quality of our numerical approximation, we compute a reference solution using the finite element method with highly refined discretizations of 19968 triangles and 10145 nodes. Figure 7 shows the WLS-Id solutions for PDE 4 with a kernel smoothness order of $\tau = 5$, calculated for

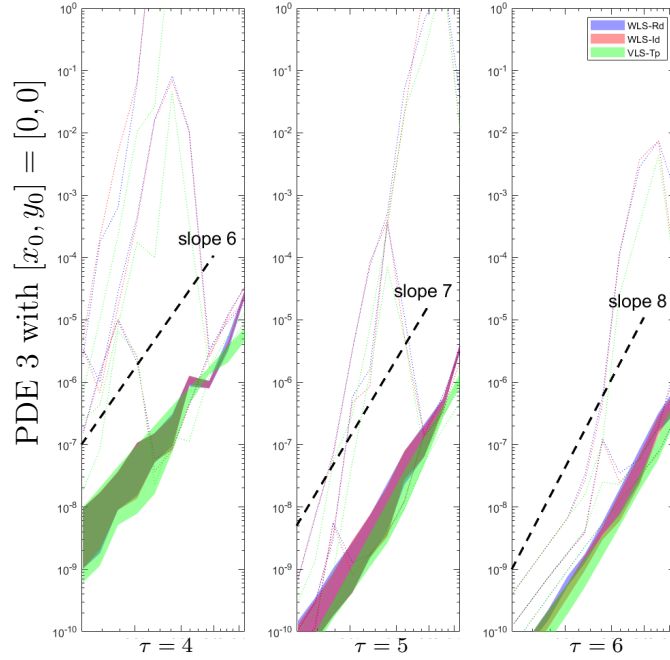


Figure 5: Relative L^2 convergence profiles for Example 2, solving the modified Helmholtz equation $\Delta u - u = f$ with a Gaussian function centered at $[0, 0]$ as the exact solution, presented in the same format as in Figure 3.

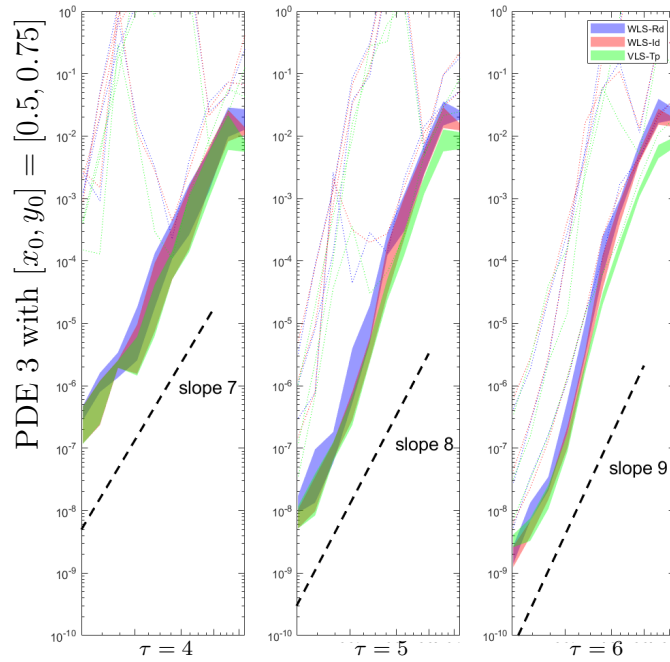


Figure 6: Relative L^2 convergence profiles for the same equation as in Figure 5 but with the Gaussian function centered at $[0.5, 0.75]$.

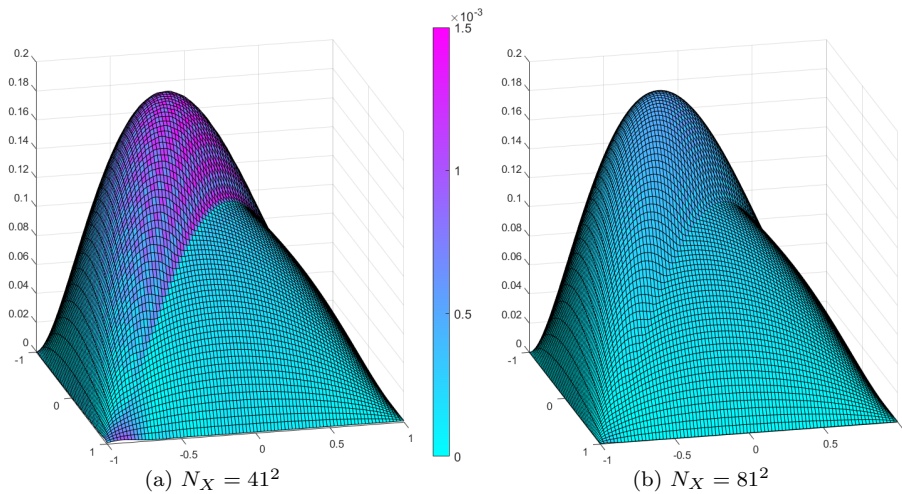


Figure 7: WLS-Id solutions for PDE 4 with kernel smoothness order $\tau = 5$ for (a) $N_X = 41^2$ and (b) 81^2 . The color map represents the absolute difference between the computed WLS-Id solution and the reference solution obtained with a highly refined finite element method.

$N_X = 41^2$ and 81^2 with surface color based on the absolute difference between the WLS-Id solution and the reference solution. We use a single color range determined by $N_X = 41^2$ in both subfigures for easy comparison. In these runs, (N_Y, N_{Y_1}, N_Z) are $(18154, 10816, 412)$ and $(48954, 41515, 812)$ for $N_X = 41^2$ and $N_X = 81^2$ respectively. Even though there are relatively fewer collocation points on the boundary (which can often lead to lower accuracy), this fact does not cause significant accuracy problems.

6. Conclusion

In this paper, we have presented a comprehensive theoretical analysis of variational and weighted least-squares kernel-based methods, filling a significant gap in the existing literature. We provided rigorous proofs for two stability inequalities, crucial for understanding the convergence behavior of these methods. Our work demonstrated that exact quadrature weights play a non-essential role in convergence and the accuracy of the solutions is not sensitive to the ratio of interior to boundary collocation points. These theoretical findings were supported by a series of numerical experiments, which showcased the efficiency and accuracy of these methods on data sets with sufficiently large mesh ratios. The results confirmed our theoretical predictions

regarding the performance of the variational method, the kernel-based collocation method, and our novel weighted least-squares collocation method. In all cases, we observed similar performance in variational and weighted least-squares kernel-based methods when the oversampling ratio was large.

Acknowledgement

This work was supported by the General Research Fund (GRF No. 12301419, 12301520, 12301021) of Hong Kong Research Grant Council, the Opening Project of Guangdong Province Key Laboratory of Computation Science at the Sun Yat-sen University (Project No. 2021014), National Natural Science Foundation of China (NSFC No. 12361086, 12001261, 12371379), Jiangxi Provincial Natural Science Foundation (No. 20212BAB211020) and Changsha Natural Science Foundation (Project No. KQ2202069).

References

- [1] E. J. Kansa, Multiquadrics—a scattered data approximation scheme with applications to computational fluid-dynamics. I. Surface approximations and partial derivative estimates, *Comput. Math. Appl.* 19 (8-9) (1990) 127–145.
- [2] Y. C. Hon, R. Schaback, On unsymmetric collocation by radial basis functions, *Appl. Math. Comput.* 119 (2-3) (2001) 177–186.
- [3] L. Ling, R. Opfer, R. Schaback, Results on meshless collocation techniques, *Eng. Anal. Bound. Elem.* 30 (4) (2006) 247–253.
- [4] L. Ling, R. Schaback, Stable and convergent unsymmetric meshless collocation methods, *SIAM J. Numer. Anal.* 46 (3) (2008) 1097–1115.
- [5] R. Schaback, All well-posed problems have uniformly stable and convergent discretizations, *Numer. Math.* 132 (2016) 597–630.
- [6] K. C. Cheung, L. Ling, R. Schaback, \mathcal{H}^2 -convergence of least-squares kernel collocation methods, *SIAM J. Numer. Anal.* 56 (1) (2018) 614–633.
- [7] S. Seyednazari, M. Tatari, D. Mirzaei, Error and stability estimates of a least-squares variational kernel-based method for second order elliptic PDEs, *Comput. Math. Appl.* 103 (2021) 1–11.

- [8] J. Jost, *Partial differential equations*, Graduate texts in mathematics, Springer, New York, 2007.
- [9] S. Agmon, A. Douglis, L. Nirenberg, Estimates near the boundary for solutions of elliptic partial differential equations satisfying general boundary conditions II, *Commun. Pure Appl. Math.* 17 (1964) 35–92.
- [10] R. Arcangéli, M. C. L. de Silanes, J. J. Torrens, Extension of sampling inequalities to Sobolev semi-norms of fractional order and derivative data, *Numer. Math.* 121 (3) (2012) 587–608.
- [11] T. Wenzel, Sharp inverse statements for kernel interpolation (2024). [arXiv:2306.14618](https://arxiv.org/abs/2306.14618).
URL <https://arxiv.org/abs/2306.14618>
- [12] S. De Marchi, R. Schaback, H. Wendland, Near-optimal data-independent point locations for radial basis function interpolation, *Advances in Computational Mathematics* 23 (3) (2005) 317–330. doi: 10.1007/s10444-004-1829-1.
- [13] T. März, C. B. Macdonald, Calculus on surfaces with general closest point functions, *SIAM J. Numer. Anal.* 50 (6) (2012) 3303–3328.
- [14] K. C. Cheung, L. Ling, A kernel-based embedding method and convergence analysis for surfaces PDEs, *SIAM J. Sci. Comput.* 40 (1) (2018) A266–A287.
- [15] M. Chen, L. Ling, Extrinsic meshless collocation methods for PDEs on manifolds, *SIAM J. Num. Anal.* 58 (2) (2020) 988–1007.
- [16] E. Fuselier, T. Hangelbroek, F. Narcowich, J. Ward, G. Wright, Localized bases for kernel spaces on the unit sphere, *SIAM J. Numer. Anal.* 51 (5) (2013) 2538–2562.
- [17] G. Santin, R. Schaback, Approximation of eigenfunctions in kernel-based spaces, *Adv. Comput. Math.* 42 (4) (2016) 973–993.
- [18] E. J. Fuselier, G. B. Wright, Scattered data interpolation on embedded submanifolds with restricted positive definite kernels: Sobolev error estimates, *SIAM J. Numer. Anal.* 50 (3) (2012) 1753–1776.

- [19] F. J. Narcowich, J. D. Ward, H. Wendland, Sobolev bounds on functions with scattered zeros, with applications to radial basis function surface fitting, *Math. Comp.* 74 (250) (2005) 743–763.
- [20] T. Tang, M. R. Trummer, Boundary layer resolving pseudospectral methods for singular perturbation problems, *SIAM J. Sci. Comput.* 17 (2) (1996) 430–438.
- [21] P. K. Mishra, Nodelab: A matlab package for meshfree node-generation and adaptive refinement, *J. Open Source Softw.* 4 (40) (2019) 1173.
- [22] R. Schaback, Superconvergence of kernel-based interpolation, *J. Approx. Theory* 235 (2018) 1–19.